University of Nebraska - Lincoln

DigitalCommons@University of Nebraska - Lincoln

Faculty Publications from the Department of Electrical and Computer Engineering

Electrical & Computer Engineering, Department of

2019

Longitudinal Phonon Plasmon Mode Coupling in β-Ga_2O_3

Mathias Schubert
University of Nebraska-Lincoln, schubert@engr.unl.edu

Alyssa Mock
University of Nebraska-Lincoln, alyssalynnmock@gmail.com

Rafal Korlacki
University of Nebraska-Lincoln, rkorlacki2@unl.edu

Sean Knight
University of Nebraska-Lincoln, seanknight@unomaha.edu

Zbigniew Galazka
Leibniz-Institut für Kristallzüchtung

See next page for additional authors

Follow this and additional works at: https://digitalcommons.unl.edu/electricalengineeringfacpub

Part of the Condensed Matter Physics Commons, and the Electrical and Computer Engineering Commons

Schubert, Mathias; Mock, Alyssa; Korlacki, Rafal; Knight, Sean; Galazka, Zbigniew; Wagner, Günther; Wheeler, Virginia; Tadjer, Marko; Goto, Ken; and Darakchieva, Vanya, "Longitudinal Phonon Plasmon Mode Coupling in β-Ga_2O_3" (2019). *Faculty Publications from the Department of Electrical and Computer Engineering*. 672.
https://digitalcommons.unl.edu/electricalengineeringfacpub/672

This Article is brought to you for free and open access by the Electrical & Computer Engineering, Department of at DigitalCommons@University of Nebraska - Lincoln. It has been accepted for inclusion in Faculty Publications from the Department of Electrical and Computer Engineering by an authorized administrator of DigitalCommons@University of Nebraska - Lincoln.

Authors

Mathias Schubert, Alyssa Mock, Rafal Korlacki, Sean Knight, Zbigniew Galazka, Günther Wagner, Virginia Wheeler, Marko Tadjer, Ken Goto, and Vanya Darakchieva

This article is available at DigitalCommons@University of Nebraska - Lincoln: https://digitalcommons.unl.edu/electricalengineeringfacpub/672

Applied Physics Letters

Longitudinal phonon plasmon mode coupling in #-Ga_2O_3

Cite as: Appl. Phys. Lett. **114**, 102102 (2019); https://doi.org/10.1063/1.5089145
Submitted: 16 January 2019 . Accepted: 18 February 2019 . Published Online: 12 March 2019

Mathias Schubert, Alyssa Mock, Rafał Korlacki, Sean Knight, Zbigniew Galazka, Günther Wagner, Virginia Wheeler, Marko Tadjer, Ken Goto, and Vanya Darakchieva

COLLECTIONS

EP This paper was selected as an Editor's Pick

View Online Export Citation CrossMark

© 2019 Author(s).

Applied Physics Letters ARTICLE scitation.org/journal/apl

Longitudinal phonon plasmon mode coupling in β-Ga_2O_3

Cite as: Appl. Phys. Lett. **114**, 102102 (2019); doi: 10.1063/1.5089145
Submitted: 16 January 2019 · Accepted: 18 February 2019 ·
Published Online: 12 March 2019

View Online Export Citation CrossMark

Mathias Schubert,[1,2,3,a)] Alyssa Mock,[3] Rafał Korlacki,[1] Sean Knight,[1] Zbigniew Galazka,[4] Günther Wagner,[4] Virginia Wheeler,[5] Marko Tadjer,[5] Ken Goto,[6] and Vanya Darakchieva[3]

AFFILIATIONS

[1]Department of Electrical and Computer Engineering, University of Nebraska-Lincoln, Lincoln, Nebraska 68588, USA
[2]Leibniz Institute for Polymer Research, Dresden 01069, Germany
[3]Terahertz Materials Analysis Center and Center for III-N technology, C3Nit - Janzén, Department of Physics, Chemistry and Biology, Linköping University, SE 58183 Linköping, Sweden
[4]Leibniz-Institut für Kristallzüchtung, Berlin 12489, Germany
[5]United States Naval Research Laboratory, Washington, DC 20375, USA
[6]Novel Crystal Technology, Inc., Sayama, Saitama-ken 350-1328, Japan

[a)]**Electronic mail:** schubert@engr.unl.edu. **URL:** http://ellipsometry.unl.edu

ABSTRACT

In this letter, we investigate a set of *n*-type single crystals of monoclinic symmetry β-Ga_2O_3 with different free electron concentration values by generalized far infrared and infrared spectroscopic ellipsometry. In excellent agreement with our previous model prediction, we find here by experiment that longitudinal-phonon-plasmon coupled modes are polarized either within the monoclinic plane or perpendicular to the monoclinic plane. As predicted, all modes change the amplitude and frequency with the free electron concentration. The most important observation is that all longitudinal-phonon-plasmon coupled modes polarized within the monoclinic plane continuously change their direction as a function of free electron concentration.

Published under license by AIP Publishing. https://doi.org/10.1063/1.5089145

The single crystalline form of gallium (III) oxide with a monoclinic crystal structure, β-Ga_2O_3, has gained substantial interest most recently for its potential use in high voltage electronic applications.[1,2] Its direct bandgap is very large, reported in a range of 4.8 eV to 5.04 eV.[3–8] A breakdown electric field of more than double of the theoretical limits for SiC and GaN is predicted, which would result in more than triple their power device performance.[2] Applications as transparent electrodes,[9] smart windows,[10,11] photovoltaic cells,[10] and gas sensors have been reported.[12] It was shown recently that β-Ga_2O_3 has the highest lifetime optical damage performance of any conductive material measured to date, above 10 J/cm^2 (1.4 GW/cm^2).[13] Very importantly, single crystalline high-quality β-Ga_2O_3 can be grown with a wide range of *n*-type conductivities, from $\approx 1 \times 10^{15}$ cm^{-3} to $\approx 1 \times 10^{20}$ cm^{-3} by unintentional or intentional donor doping in bulk and epitaxial materials.[2] Correct and accurate characterization of free charge carrier properties in bulk and heteroepitaxial layer structures is a crucial step in the successful design of semiconductor heterostructure devices. Long-wavelength (infrared and farinfrared) optical spectroscopy, in particular ellipsometry, is a traditional tool to investigate the effect of free charge carriers on the optical response of semiconductor materials, even if part of complex layer structures.[14] At long wavelengths, specifically in materials with polar lattice resonances, collective free charge carrier excitations, plasmons, couple with the lattice vibration modes.[15–17] This effect and related phenomena observable in optical spectroscopies are well known for materials with crystal symmetries higher than or equal to orthorhombic, for example, in the zincblende-structure (cubic) GaAs,[18] InSb,[19] InAs,[19] or the wurtzite-structure (hexagonal) CdS,[20] ZnO,[21] GaN,[22,23] InN,[24] or the rutile-structure (tetragonal) SnO_2.[25] In all such cases, coupling of longitudinal optical (LO) phonons with collective plasma oscillations (plasmons) occurs along high-symmetry directions of the lattice. The coupled modes, while changing their frequencies, with the increasing free charge carrier density maintain the polarization direction of the LO phonons at zero free charge carrier density. In semiconductors with monoclinic symmetry, such as β-Ga_2O_3, plasmons also couple with LO phonons. In our recent work, we have shown that LO phonons within the monoclinic plane of β-Ga_2O_3 are not polarized parallel to any of the low-index crystallographic directions.[26] Instead, their

Published under license by AIP Publishing

directions, at first sight, appear to be randomly distributed. However, upon closer inspection, it becomes clear that the LO mode directions are tied to the specific values of all amplitude, direction, and frequency parameters of all transverse optical (TO) lattice modes.[27] We have further identified that LO modes are affected by free charge carriers and form longitudinal-phonon-plasmon (LPP) coupled modes. In Ref. 26, we hypothesized about the behavior of the LPP modes as a function of the free charge carrier density, and we predicted that all eigendielectric displacement directions of the LPP modes would vary with free charge carrier density. We also hypothesized that the order of the LPP modes with respect to the TO modes would change. However, in our previous work,[26] only specimens with approximately the same free electron density were investigated, and the variation of LPP modes with free electron density remained experimentally unexplored. Verification of LPP mode properties is important, for example, to reliably calculate effects of electron-phonon interaction and high electric fields on electronic transport properties.[28–31] In this letter, we present the result of an investigation of LPP modes in a set of samples with free electron density parameters varying from $\approx 5 \times 10^{17}\,\mathrm{cm}^{-3}$ to $\approx 6 \times 10^{18}\,\mathrm{cm}^{-3}$.

The derivations of the LPP mode parameters and the phonon mode order in monoclinic crystals follow closely the original reports in Refs. 26 and 27, respectively, which is due to the fact that space limitations are kept minimal here. The long wavelength dependencies of the dielectric function tensor, $\varepsilon(\omega)$, and the dielectric loss function tensor, $\varepsilon^{-1}(\omega)$, can be described by two sets of eigenmodes—the TO and LO phonon modes—and wavelength independent polarizability contributions (ε_∞) due to electronic and excitonic excitations at photon energies much higher than all lattice mode frequencies.[16,17,32] TO modes occur at frequencies at which dielectric resonance occurs for electric fields along $\hat{\mathbf{e}}_l$ with eigendielectric displacement unit vectors then defined as $\hat{\mathbf{e}}_l = \hat{\mathbf{e}}_{\mathrm{TO},l}$.[33] Similarly, LO modes occur when the dielectric loss approaches infinity for electric fields along $\hat{\mathbf{e}}_l$ with eigendielectric displacement unit vectors then defined as $\hat{\mathbf{e}}_l = \hat{\mathbf{e}}_{\mathrm{LO},l}$.[16] An eigendielectric displacement vector summation (EDVS) approach was introduced recently,[26,27,34,35] where ε is composed of sums of dyadics, $(\hat{\mathbf{e}}_{\mathrm{TO},l} \otimes \hat{\mathbf{e}}_{\mathrm{TO},l})$, scaled with frequency-dependent complex-valued response functions, $\varrho_{\mathrm{TO},l}$

$$\varepsilon = \varepsilon_\infty + \sum_{l=1}^{N} \varrho_{\mathrm{TO},l}(\hat{\mathbf{e}}_{\mathrm{TO},l} \otimes \hat{\mathbf{e}}_{\mathrm{TO},l}), \tag{1}$$

where the index l denotes all TO modes within the monoclinic lattice. In the absence of doping, β-Ga_2O_3 possesses 8 B_u-symmetry TO modes polarized within the monoclinic lattice plane and 4 A_u-symmetry TO modes polarized parallel to the lattice axis b. The inverse of ε is obtained by an eigendielectric displacement loss vector summation (EDLVS) approach[36]

$$\varepsilon^{-1} = \varepsilon_\infty^{-1} - \sum_{l=1}^{N} \varrho_{\mathrm{LO},l}(\hat{\mathbf{e}}_{\mathrm{LO},l} \otimes \hat{\mathbf{e}}_{\mathrm{LO},l}), \tag{2}$$

where the index l denotes all LO modes within the monoclinic lattice. Anharmonically broadened Lorentzian oscillator functions can be used to describe functions ϱ in Eqs. (1) and (2)

$$\varrho_{k,l}(\omega) = \frac{A_{k,l}^2 - i\Gamma_{k,l}\omega}{\omega_{k,l}^2 - \omega^2 - i\omega\gamma_{k,l}}. \tag{3}$$

Here, $A_{k,l}$, $\omega_{k,l}$, $\gamma_{k,l}$, and $\Gamma_{k,l}$ denote the amplitude, resonance frequency, harmonic broadening, and anharmonic broadening parameters for TO ($k =$ "TO") or LO ($k =$ "LO") mode l, respectively, and ω is the frequency of the driving electromagnetic field. We note a misprint in Eq. (10) of Ref. 26 where the square on the amplitude parameter was erroneously omitted.

The contributions of free charge carriers to ε are augmented using the Drude model for free charge carriers.[14] In order to account for the three dimensional nature of the motion of free charge carriers and their directional anisotropy for transport properties (optical mobility parameters), free charge carrier contributions are augmented by 3 additional terms to Eq. (1)

$$\varepsilon_{\mathrm{LPP}} = \varepsilon + \sum_{l=1}^{3} \varrho_{\mathrm{TO}=0,l}(\hat{\mathbf{e}}_{\mathrm{TO}=0,l} \otimes \hat{\mathbf{e}}_{\mathrm{TO}=0,l}). \tag{4}$$

We select directions $\hat{\mathbf{e}}_{\mathrm{TO}=0,l}$ to coincide with Cartesian coordinate axes (x, y, z). The definition of the Cartesian axes with respect to the crystal unit cell of β-Ga_2O_3 is described in the supplementary material. Briefly, crystal axes a and c are within the monoclinic plane, and axis b is perpendicular to the monoclinic plane. **a** is parallel to x, **b** is antiparallel to z, and **c** is within the (x, y) plane. $\varrho_{\mathrm{TO}=0,l}$ can be expressed as follows:

$$\varrho_{\mathrm{TO}=0,(x,y,z)} = -\frac{e^2 N}{\tilde{\varepsilon}_0 m^\star_{(x,y,z)} m_e \omega(\omega + i\gamma_{\mathrm{P},(x,y,z)})}, \tag{5}$$

where N is the free charge carrier volume density parameter, e is the electronic charge, m_e is the free electron mass, $m^\star_{(x,y,z)}$ are the three directional effective mass parameters, and the directional plasma broadening parameters $\gamma_{\mathrm{P},(x,y,z)}$ are connected with the directional optical mobility parameters

$$\mu_{(x,y,z)} = \frac{e}{\tilde{\varepsilon}_0 m^\star_{(x,y,z)} m_e \gamma_{\mathrm{P},(x,y,z)}}. \tag{6}$$

The plasma frequency parameter is then also dependent on the polarization direction

$$\omega^2_{\mathrm{P},(x,y,z)} = \frac{e^2 N}{m^\star_{(x,y,z)} m_e}, \tag{7}$$

and can be considered as an isotropic value when the effective mass parameters are isotropic. For β-Ga_2O_3, it was found in recent optical Hall effect measurements that the bottom conduction band effective mass parameter is isotropic and $m^\star_x = m^\star_y = m^\star_z = 0.28$.[37]

Analogously, three terms are added for ε^{-1}

$$\varepsilon^{-1}_{\mathrm{LPP}} = \varepsilon^{-1} - \sum_{l=1}^{N+3} \varrho_{\mathrm{LPP},l}(\hat{\mathbf{e}}_{\mathrm{LPP},l} \otimes \hat{\mathbf{e}}_{\mathrm{LPP},l}). \tag{8}$$

We note that while the addition of 3 Drude terms to Eq. (1) does not change the TO mode parameters, all LO mode parameters change in Eq. (2) upon the addition of the three terms in Eq. (8) reflecting the LPP mode coupling. For polarization within the monoclinic plane, i.e., modes with B_u-symmetry, and for a single species free charge carrier density (such as single band holes, or single band electrons) two TO modes with zero frequency $\omega_{\mathrm{TO}} = 0$ must be added to Eq. (4), hence, 10 TO modes exist, and 10 associated LPP modes must occur in Eq.

Published under license by AIP Publishing

(8), oriented (polarized) within the monoclinic **a**–**c** plane. For polarization perpendicular to the monoclinic plane, i.e., modes with A_u-symmetry, one TO mode with zero frequency ω_{TO} is added to Eq. (4), and hence, the displacement directions of 5 TO modes and 5 associated LPP modes (A_u symmetry) are oriented perpendicular to the monoclinic plane. Thus, all eigenvectors are aligned with axis b. Hence, for B_u- and A_u-symmetry LPP modes, $\hat{\mathbf{e}}_{LPP,l} = \cos\alpha_{LPP,l}\hat{\mathbf{x}} + \sin\alpha_{LPP,l}\hat{\mathbf{y}}$ and $\hat{\mathbf{e}}_{LPP,l} = -\hat{\mathbf{z}}$, respectively. Thereby, we have introduced the parameters $\alpha_{LPP,l}$ representing the directions of the LPP modes. The directions can be determined as a function of the electron density or, equivalently, ω_p. After setting all broadening parameters in Eqs. (3) and (5) to zero, the LPP mode parameters $\omega_{LPP,l}$, $\alpha_{LPP,l}$, and $A_{LPP,l}$ follow from the following relations, respectively (also see supplementary material),[26,34]

$$\det\{\varepsilon_{LPP}(\omega = \omega_{LPP,l})\} \to 0, \tag{9}$$

$$\varepsilon_{LPP}(\omega = \omega_{LPP,l})\hat{\mathbf{e}}_{LPP,l} = 0, \tag{10}$$

$$(\varepsilon_{LPP})^{-1} = \varepsilon_{LPP}^{-1}. \tag{11}$$

We have performed a series of long-wavelength ellipsometry measurements on a set of different bulk single crystals with various

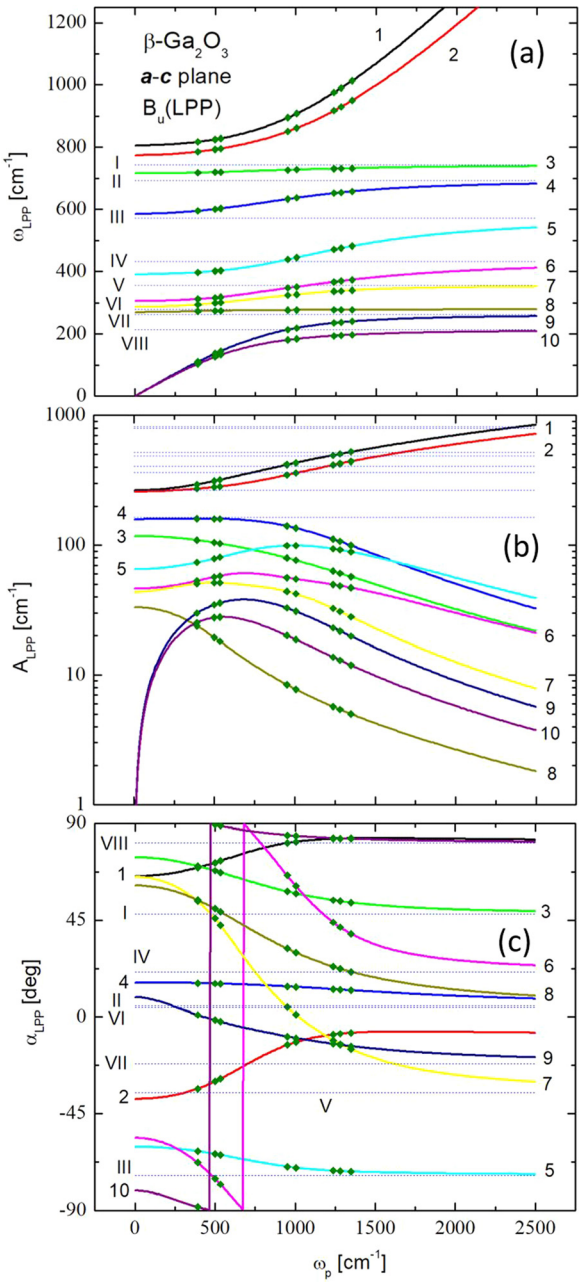

FIG. 1. B_u-symmetry LPP mode parameters as a function of ω_p, (a) frequency, (b) amplitude, and (c) angular direction relative to axis a within the **a**–**c** plane. The horizontal lines and roman numerals indicate the corresponding parameters of the TO modes. The symbols (diamonds) indicate the results from the experiment obtained in this work. Numerical data are given in the supplementary material.

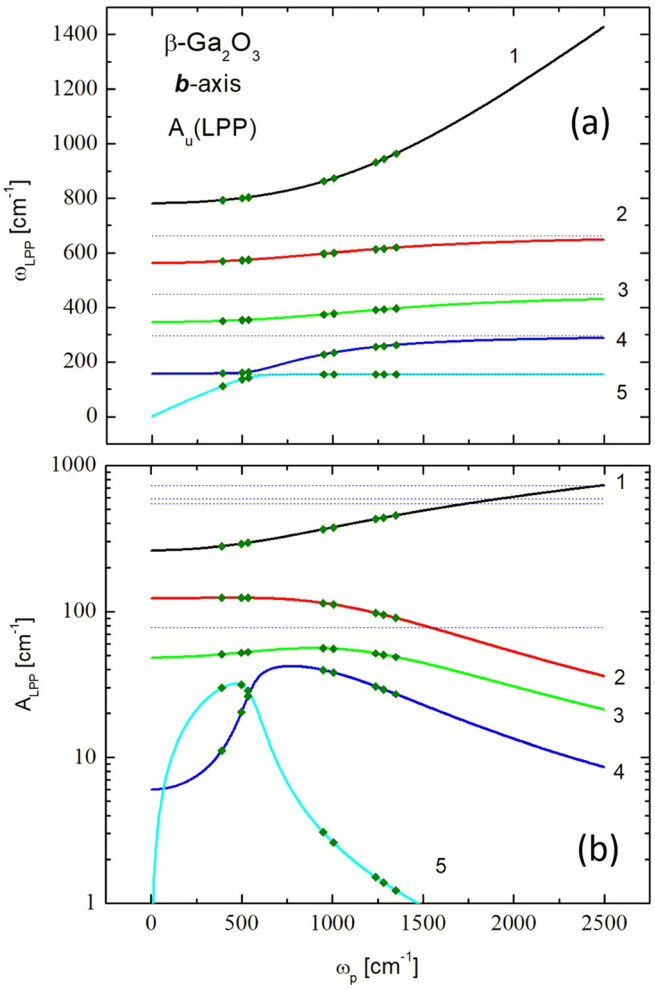

FIG. 2. A_u-symmetry LPP mode parameters as a function of ω_p, (a) frequency and (b) amplitude. Note that all angular parameters are parallel to axis b. The horizontal lines indicate the corresponding parameters of the TO modes. The symbols (diamonds) indicate the results from the experiment obtained in this work. Numerical data are given in the supplementary material.

Published under license by AIP Publishing

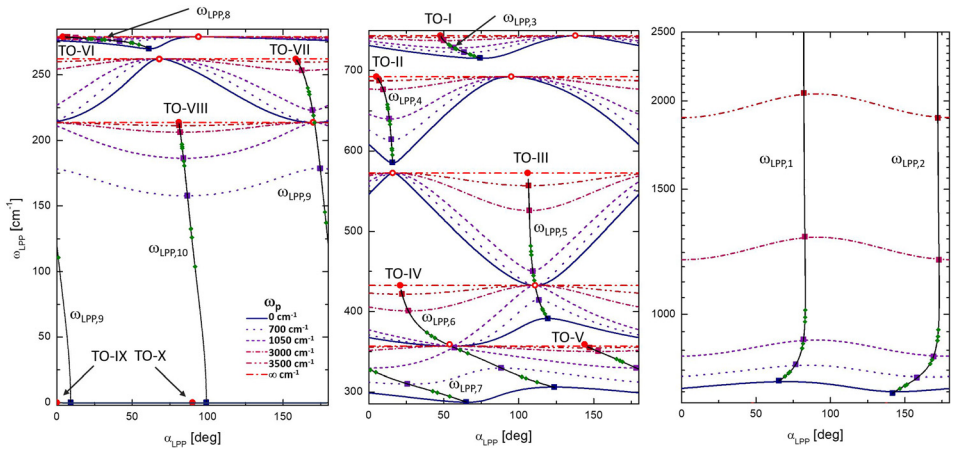

FIG. 3. Colored lines with different styles: B_u-symmetry directional limiting frequencies, $\omega(\alpha)_{LPP,l}$, for β-Ga_2O_3 as a function of displacement direction, α, relative to axis a within the monoclinic plane, for selected plasma frequency parameters (see the inset for labels). The black solid lines indicate the evolution of LPP modes as a continuous function of ω_p. The square symbols indicate the B_u-symmetry LPP modes. Left panel: modes $\omega(\alpha)_{LPP,8}$-$\omega(\alpha)_{LPP,10}$, middle panel: modes $\omega(\alpha)_{LPP,3}$-$\omega(\alpha)_{LPP,7}$, and right panel: modes $\omega(\alpha)_{LPP,1}$ and $\omega(\alpha)_{LPP,2}$. Note the different *y* axis scales. The full red circles and numerals indicate B_u-symmetry TO modes. The open red circles indicate the TO frequencies at orientations perpendicular to the lattice TO mode polarization. The green diamonds indicate the experimental data observed in this work for LPP modes.

surface orientations and different free electron density parameters. The details of the experimental procedures and sample descriptions are given in Ref. 26 and the supplementary material, respectively. The selected experimental and best-model calculated ellipsometry data are shown in the supplementary material and omitted here for brevity. We have analyzed all ellipsometry data by using the model dielectric function tensor approach discussed in Ref. 26. We have analyzed data from every sample separately. As a result, we determined the best-match model calculated plasma frequency parameter and the mobility parameters for all three major axes directions, **a**, **c***, and **b**. The results for the mobility parameters are not further discussed here. The LPP mode parameters are calculated from the best-match model calculated dielectric function tensor after setting all the phonon mode and plasma broadening parameters to zero. The results of the LPP mode parameters are included in Figs. 1, 2, and 3, which are discussed below.

Figures 1(a)–1(c) depict the dependencies of the LPP mode parameters as a function of ω_p. The solid lines in Figs. 1(a)–1(c) are calculated with the phonon mode parameters determined in Ref. 26. The symbols in Figs. 1(a)–1(c) indicate the parameters obtained from set of samples investigated by ellipsometry in this work. An excellent match between the hypothesized behavior (solid lines) and the experimental observation (symbols) is noted. At small ω_p, 2 additional LPP branches emerge from zero [labeled 9 and 10 in Figs. 1(a)–1(c)], polarized within the monoclinic plane. With increasing ω_p, the LPP frequencies [Fig. 1(a)] shift away from their originating LO modes at $\omega_p = 0$. The phonon mode order changes gradually, whereby the frequencies of B_u-LPP modes 5, 6, and 9 cross frequencies of TO modes IV, V, and VIII [Fig. 1(a)], respectively. Such an occurrence is never observed for semiconductors with symmetry higher than monoclinic. The two highest B_u-LPP branches approach infinity for $\omega_p \to \infty$. The amplitude parameters reflect the coupling behavior between LO and plasmon modes. The two additional modes, labeled 9 and 10, represent the plasmon-like behavior for small ω_p. Also note the linear increase for their frequencies. For intermediate carrier densities, all amplitudes begin to diminish, except for the 2 modes with the largest frequencies, labeled 1 and 2. These are the plasmon-like modes for very large ω_p. Accordingly, while all amplitudes of all other modes approach zero eventually, the amplitudes of modes labeled 1 and 2 approach infinity for $\omega_p \to \infty$. Figure 1(c) depicts the evolution of the LPP angular orientation, which represents the displacement direction of the associated lattice motion.[38] In contrast to the behavior of LPP modes in semiconductors with symmetry higher than monoclinic, the LPP mode lattice displacement directions continuously shift with increasing ω_p. For very large ω_p, all directions approach eventually one of the TO mode displacement directions. This variation is not random and will be addressed further below.

Figures 2(a) and 2(b) depicts the same as Figs. 1(a)–1(c) for the A_u-LPP modes. An excellent match between the hypothesized behavior (solid lines) and the experimental observation (symbols) is noted. The behavior observed here is very similar to LPP mode coupling in semiconductors with multiple phonon mode branches and symmetries higher than monoclinic. At small ω_p, one additional branch emerges from zero. With increasing ω_p, the LPP modes shift away from their associated LO mode frequencies at $\omega_p = 0$, but do not change the phonon mode order. The highest frequency mode approaches infinity for $\omega_p \to \infty$. Likewise, the amplitude of the highest LPP mode approaches infinity for a very large plasma frequency, while all other amplitudes approach zero.

Within the Born and Huang approach,[33] which permits the calculation of the lattice dynamic properties in crystals with arbitrary symmetry, solutions with $\mathbf{E} \neq 0$ and $\mathbf{D} \neq 0$ define the so-called limiting frequencies $\omega(\alpha)_l$.[39] Here, α parameterizes the lattice displacement direction of $\omega(\alpha)_l$ within the monoclinic plane. We recently showed that $\omega(\alpha)_l$ can be determined from analysis of experimental ellipsometry data, and we provided an explanation for the order of all TO, LO, and $\omega(\alpha)_l$ modes in crystals with monoclinic symmetry without free charge carriers.[27] In the case of LPP mode coupling, modes $\omega(\alpha)_l$ also couple and may be termed $\omega(\alpha)_{LPP,l}$. Figure 3 depicts $\omega(\alpha)_{LPP,l}$ for different values of ω_p. For $\omega_p = 0$, Fig. 3 is identical to Fig. 1(c) in Ref. 27, which is explained there in detail. Here, we demonstrate the effect of plasmon coupling.

Published under license by AIP Publishing

Modes $\omega(\alpha)_{\mathrm{LPP},l}$ in Fig. 3 are bound between TO and LPP modes. LPP modes shift with ω_{p}, and $\omega(\alpha)_{\mathrm{LPP},l}$ changes accordingly. There are 10 modes of $\omega(\alpha)_{\mathrm{LPP},l}$, bound within pairs of 10 TO and 10 LPP modes, and the order remains to be discussed in detail. Briefly, we note that the lowest-frequency mode, $\omega(\alpha)_{\mathrm{LPP},10}$, is bound between the zero-frequency modes TO-IX and TO-X (the Drude contributions). The highest-frequency mode, $\omega(\alpha)_{\mathrm{LPP},1}$, is bound between LPP-1 and LPP-2, and all approach infinity when $\omega_{\mathrm{p}} \rightarrow \infty$. Also shown here are the experimental data obtained in this work. Included in Fig. 3 are the LPP modes with ω_{p} (black solid lines). At $\omega_{\mathrm{p}} = 0$, all LPP modes emerge from an LO mode, recognizing that the Drude contributions for $\omega_{\mathrm{p}} = 0$ originate from two LO modes with zero frequency. All LPP modes are further bound by a TO mode, except for the two highest frequency modes which approach infinity. It is an interesting thought to consider the frequency at infinity as the virtual TO modes for the Drude contributions, which appear in reality at zero frequency. We further observe again that LPP modes 5, 6, and 9 cross frequencies of TO modes IV, V, and VIII, respectively. In Fig. 3, it can now be seen clearly that the crossings appear with a polarization direction of the respective LPP mode, and the polarization direction of the respective LPP at the crossing is perpendicular to the polarization direction of the TO mode being crossed.

The free charge carrier density parameters obtained from our ellipsometry analysis and the nominal free electron density parameters, $N_d - N_a$, provided by the crystal growers are given in the supplementary material. We note very good to excellent agreement. Note that all electrical Hall measurements were performed on different pieces from those investigated here but cut from the same bulk crystals. Due to gradients in defect and dopant densities across the Czochralski grown crystals, occasional deviations seen between our optical results and those reported from electrical investigations are therefore not unexpected.

See supplementary material for the details of the samples investigated, the experimental procedures, and the numerical values of all the parameters determined in this work.

This work was supported in part by the National Science Foundation under Award No. DMR 1808715, the Air Force Office of Scientific Research under Award No. FA9550-18-1-0360, the Nebraska Materials Research Science and Engineering Center under Award No. DMR 1420645, the Swedish Energy Agency under Award No. P45396-1, the Swedish Research Council VR Award No. 2016-00889, the Swedish Foundation for Strategic Research Grant Nos. FL12-0181, RIF14-055, and EM16-0024, and the Swedish Government Strategic Research Area in Materials Science on Functional Materials at Linköping University, Faculty Grant SFO Mat LiU No. 2009-00971. M.S. acknowledges the University of Nebraska Foundation and the J. A. Woollam Foundation for financial support. We acknowledge Klaus Irmscher for critical reading of this manuscript.

REFERENCES

[1] M. Higashiwaki, K. Sasaki, H. Murakami, Y. Kumagai, A. Koukitu, A. Kuramata, T. Masui, and S. Yamakoshi, Semicond. Sci. Technol. **31**, 034001 (2016).
[2] M. Higashiwaki and G. H. Jessen, Appl. Phys. Lett. **112**, 060401 (2018).
[3] C. Janowitz, V. Scherer, M. Mohamed, A. Krapf, H. Dwelk, R. Manzke, Z. Galazka, R. Uecker, K. Irmscher, R. Fornari, M. Michling, D. Schmeißer, J. R. Weber, J. B. Varley, and C. G. V. de Walle, New J. Phys. **13**, 085014 (2011).
[4] C. Sturm, R. Schmidt-Grund, C. Kranert, J. Furthmüller, F. Bechstedt, and M. Grundmann, Phys. Rev. B **94**, 035148 (2016).
[5] C. Sturm, J. Furthmüller, F. Bechstedt, R. Schmidt-Grund, and M. Grundmann, APL Mater. **3**, 106106 (2015).
[6] J. Furthmüller and F. Bechstedt, Phys. Rev. B **93**, 115204 (2016).
[7] A. Mock, R. Korlacki, C. Briley, V. Darakchieva, B. Monemar, Y. Kumagai, K. Goto, M. Higashiwaki, and M. Schubert, Phys. Rev. B **96**, 245205 (2017).
[8] Z. Galazka, Semicond. Sci. Technol. **33**, 113001 (2018).
[9] U. Betz, M. K. Olsson, J. Marthy, M. Escola, and F. Atamny, Surf. Coat. Technol. **200**, 5751 (2006).
[10] C. G. Granqvist, *Handbook of Inorganic Electrochromic Materials* (Elsevier, 1995).
[11] D. Gogova, A. Iossifova, T. Ivanova, Z. Dimitrova, and K. Gesheva, J. Cryst. Growth **198/199**, 1230 (1999).
[12] F. Réti, M. Fleischer, H. Meixner, and J. Giber, Sens. Actuators, B Chem. **19**, 573 (1994).
[13] J.-H. Yoo, S. Rafique, A. Lange, H. Zhao, and S. Elhadj, APL Mater. **6**, 036105 (2018).
[14] M. Schubert, *Infrared Ellipsometry on Semiconductor Layer Structures: Phonons, Plasmons and Polaritons*, Springer Tracts in Modern Physics Vol. 209 (Springer, Berlin, 2004).
[15] B. B. Varga, Phys. Rev. **137**, A1896 (1965).
[16] C. Kittel, *Introduction to Solid State Physics* (Wiley India Pvt. Ltd, 2009).
[17] M. Grundmann, *The Physics of Semiconductors* (Springer, Berlin Heidelberg, 2016).
[18] C. G. Olson and D. W. Lynch, Phys. Rev. **177**, 1231 (1969).
[19] N. K. S. Gaur, Physica B + C **82**, 262 (1976).
[20] R. J. Bell, T. J. McMahon, and D. G. Rathbun, J. Appl. Phys. **39**, 48 (1968).
[21] M. Göppert, F. Gehbauer, M. Hetterich, J. Münzel, D. Queck, and C. Klingshirn, J. Lumin. **72–74**, 430 (1997).
[22] P. Perlin, J. Camassel, W. Knap, T. Taliercio, J. C. Chervin, T. Suski, I. Grzegory, and S. Porowski, Appl. Phys. Lett. **67**, 2524 (1995).
[23] A. Kasic, M. Schubert, Y. Saito, Y. Nanishi, and G. Wagner, Phys. Rev. B **65**, 115206 (2002).
[24] Y. Ishitani, M. Fujiwara, X. Wang, S.-B. Che, and A. Yoshikawa, Appl. Phys. Lett. **92**, 251901 (2008).
[25] M. Feneberg, C. Lidig, K. Lange, M. E. White, M. Y. Tsai, J. S. Speck, O. Bierwagen, and R. Goldhahn, Physica Status Solidi A **211**, 82 (2014).
[26] M. Schubert, R. Korlacki, S. Knight, T. Hofmann, S. Schöche, V. Darakchieva, E. Janzén, B. Monemar, D. Gogova, Q.-T. Thieu, R. Togashi, H. Murakami, Y. Kumagai, K. Goto, A. Kuramata, S. Yamakoshi, and M. Higashiwaki, Phys. Rev. B **93**, 125209 (2016).
[27] M. Schubert, A. Mock, R. Korlacki, and V. Darakchieva, Phys. Rev. B **99**, 041201(R) (2019).
[28] K. Ghosh and U. Singisetti, Appl. Phys. Lett. **109**, 072102 (2016).
[29] K. Ghosh and U. Singisetti, J. Mater. Res. **32**, 4142 (2017).
[30] K. Ghosh and U. Singisetti, J. Appl. Phys. **122**, 035702 (2017).
[31] A. Parisini, K. Ghosh, U. Singisetti, and R. Fornari, Semicond. Sci. Technol. **33**, 105008 (2018).
[32] P. Yu and M. Cardona, *Fundamentals of Semiconductors* (Springer, Berlin, 1999).
[33] M. Born and K. Huang, *Dynamical Theory of Crystal Lattices* (Clarendon, Oxford, 1954).
[34] M. Schubert, Phys. Rev. Lett. **117**, 215502 (2016).
[35] A. Mock, R. Korlacki, S. Knight, and M. Schubert, Phys. Rev. B **95**, 165202 (2017).
[36] A. Mock, R. Korlacki, S. Knight, and M. Schubert, Phys. Rev. B **97**, 165203 (2018).
[37] S. Knight, A. Mock, R. Korlacki, V. Darakchieva, B. Monemar, Y. Kumagai, K. Goto, M. Higashiwaki, and M. Schubert, Appl. Phys. Lett. **112**, 012103 (2018).
[38] We note that modes shown in Fig. 13 in Ref. 26 were accidentally calculated with the coordinate axes x and y exchanged. Figure 1(c) in this present work depicts the correct angular orientations.
[39] G. Venkataraman, L. A. Feldkamp, and V. C. Sahni, *Dynamics of Perfect Crystals* (The MIT Press, Cambridge, Massachusetts, and London, England, 1975).

Published under license by AIP Publishing